Supporting Information

Constructing of fragmentary g-C_3N_4 framework with rich nitrogen defects as highly efficient metal-free catalyst for acetylene hydrochlorination

Xianliang Qiao,†[a] Zhiqiang Zhou,†[a] Xinyu Liu,[a] Chaoyue Zhao,[a] Qingxin Guan,*[a] Wei Li*[a,b]

[a] College of Chemistry, State Key Laboratory of Elemento-Organic Chemistry, Key Laboratory of Advanced Energy Materials Chemistry (Ministry of Education), Nankai University, Tianjin 300071, China

[b] Collaborative Innovation Center of Chemical Science and Engineering (Tianjin), Nankai University, Tianjin 300071, China

† Both authors contributed equally to this work.

*Corresponding Author. Tel.: +86-22-83662780; E-mail: qingxinguan@nankai.edu.cn (Q. Guan).

*Corresponding Author. Tel.&Fax: +86-22-23508662; E-mail: weili@nankai.edu.cn (W. Li).

Table of Contents

■ STEM image of MF-600 with elemental mapping

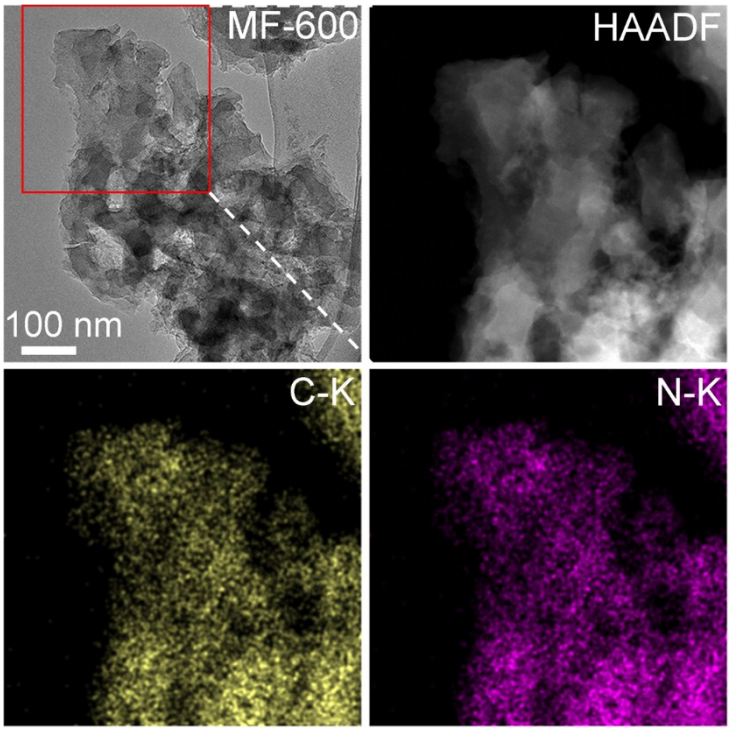

Fi. S1 STEM image of MF-600 with elemental mapping of C and N.

■ Nitrogen adsorption–desorption results of MF-x materials

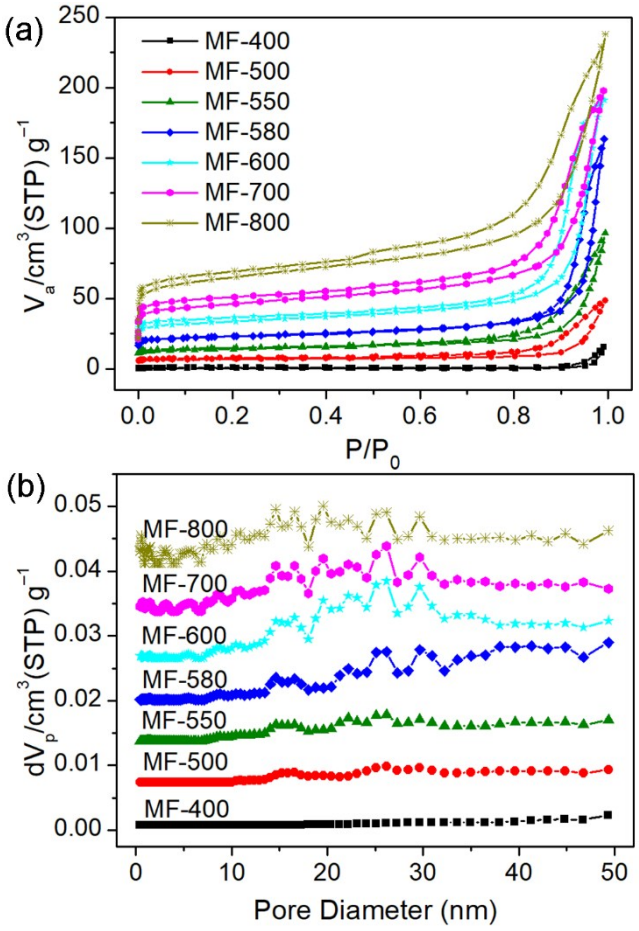

Fig. S2 (a) Nitrogen adsorption-desorption isotherms and (b) pore size distributions curves of MF-x materials.

Table S1 Textural properties of MF-x materials[a].

Sample	S_{BET} ($m^2 \cdot g^{-1}$)	V_{tot} ($cm^3 \cdot g^{-1}$)
MF-400	1.7	0.02
MF-500	6.6	0.06
MF-550	17.3	0.13
MF-580	28.8	0.23
MF-600	47.9	0.26
MF-700	93.1	0.30
MF-800	161.2	0.32

[a] S_{BET} and V_{tot} in the table represent specific surface area and total pore volume, respectively. S_{BET} was calculated by BET method, V_{tot} was estimated from the nitrogen adsorption isotherm at P/P_0=0.99.

■ EA and XPS analysis results of MF-x materials

Table S2 Compositions of C, N, H (wt.%) and C/N atomic ratios in samples determined by EA.

Sample	C (wt.%)	N (wt.%)	H (wt.%)	C/N (atomic ratio)
MF-400	40.11	50.55	2.95	0.93
MF-500	42.50	49.45	2.35	1.00
MF-550	42.85	48.72	1.94	1.03
MF-580	44.83	44.54	3.21	1.17
MF-600	47.23	38.90	2.35	1.42
MF-700	55.45	31.97	2.64	2.02
MF-800	64.73	25.00	1.61	3.02

Table S3 Compositions of C, N, O (wt.%) and C/N atomic ratios in samples determined by XPS.

Sample	C (wt.%)	N (wt.%)	O (wt.%)	C/N (atomic ratio)
MF-400	50.42	45.39	4.18	1.29
MF-500	52.25	42.84	4.91	1.31
MF-550	59.77	35.85	4.37	1.80
MF-580	61.64	31.27	7.09	2.30
MF-600	64.13	29.35	6.52	2.55
MF-700	68.22	25.62	6.16	3.11
MF-800	71.94	22.60	5.46	3.71

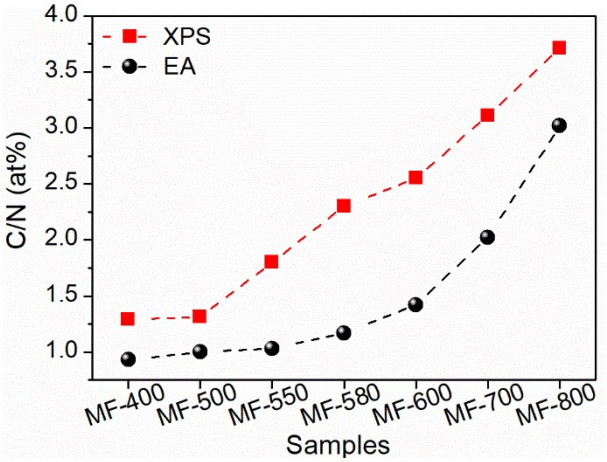

Fig. S3 C/N atomic ratio in MF-x materials determined by EA and XPS methods.

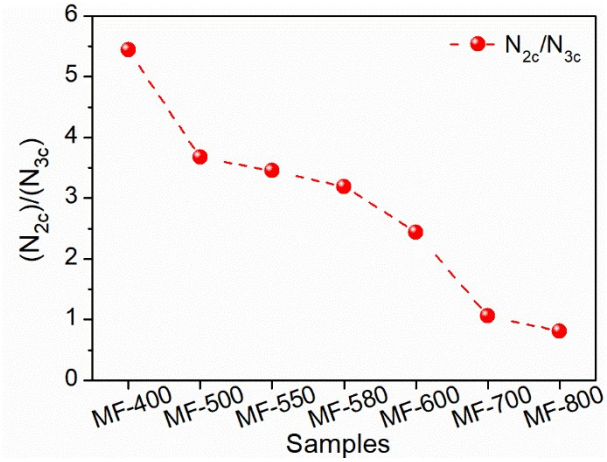

Fig. S4 N_{2c}/N_{3c} atomic ratio in MF-x materials determined by XPS analysis.

■ Structure model for pure g-C_3N_4 and fragmentary g-C_3N_4

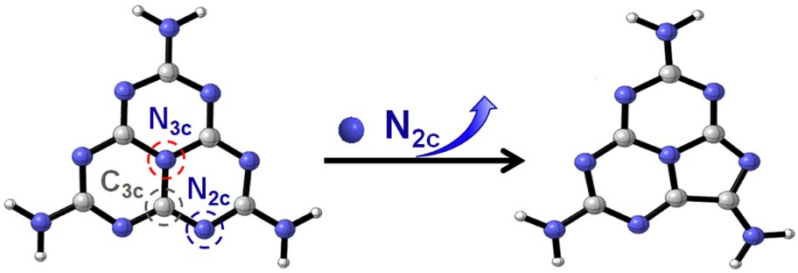

Fig. S5 Structure models for pure g-C_3N_4 and fragmentary g-C_3N_4.

■ Space-time yields (STY) of VCM over catalysts

Table S4 STY of VCM over MF-x and malemine-600 catalysts[a].

Catalyst	Temp. (°C)	Con. (%)	GHSV (h^{-1})	STY ($g_{vcm} \cdot h^{-1} \cdot g_{cat}^{-1}$)
MF-400	220	7	30	0.02
MF-500	220	20	30	0.06
MF-550	200	23	30	0.07
MF-580	220	44	30	0.08
MF-600	220	30	200	0.35
MF-700	220	31	200	0.36
MF-800	220	19	200	0.22
Melamine-600	220	3	30	0.01

[a] STY of all materials were calculated at a yield level of VCM < 45%.

Table S5 Comparison of STY of VCM between MF-600 developed in this work and other reported metal-free catalysts.

Catalyst	Temp. (°C)	Con. (%)	GHSV (h^{-1})	STY ($g_{vcm} \cdot h^{-1} \cdot g_{cat}^{-1}$)
C_3N_4/AC[S2]	180	77	50	0.25
B,N-graphene[S3]	150	95	36	0.15
NC(ZIF-8)[S4]	220	92	30	0.17
SiC@NC[S5]	200	80	30	0.10
NS-C-NH_3[S6]	220	80	35	0.68[a]
PDA-800[S7]	200	70	--	0.28
PANI-AC[S8]	180	76	36	0.16
p-BN[S9]	280	99	44	0.17
NP-C600[S1]	210	<15	200	1.81[b]
MF-600	**220**	**94**	**50**	**0.27[c]**
MF-600	**220**	**30**	**200**	**0.35[d]**

[a] Reaction was carried out with a gas pressure of 1 kPa. [b] STY of NP-C600 was calculated at a yield level of VCM < 15%. [c, d] Catalyst was developed in this work.

■ Stability test of MF-600

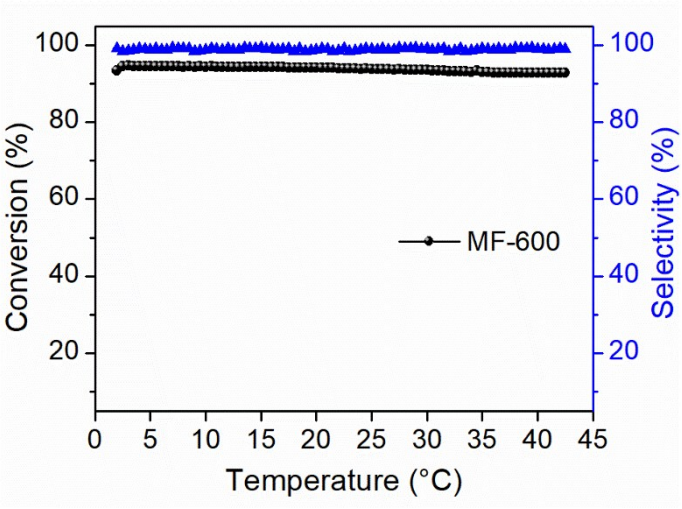

Fig. S6 Long-time testing of MF-600 under 30 h^{-1} and 220 °C.

■ Structure characterization of MF-600 and melamine-600

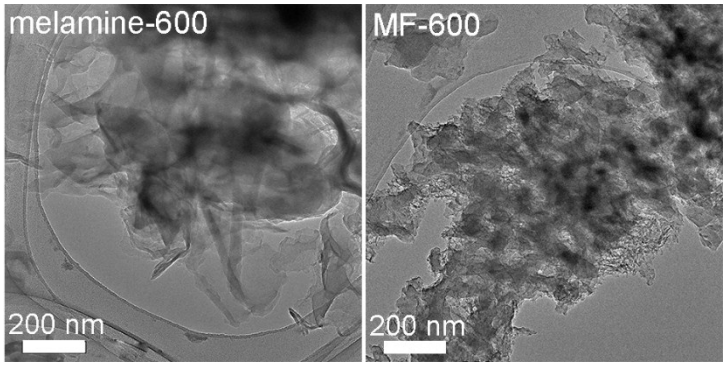

Fig. S7 TEM images of melamine-600 and MF-600.

Table S6 Characterization data of MF-600 and melamine-600 by EA, XPS and nitrogen adsorption–desorption test.

Sample	C (wt.%)[a]	N (wt.%)[a]	O (wt.%)[a]	C/N (atomic ratio)[a]	C/N (atomic ratio)[b]	S_{BET} ($m^2 \cdot g^{-1}$)[c]	V_{tot} ($cm^3 \cdot g^{-1}$)[c]
melamine-600	44.74	52.36	2.90	1.0	0.76	6.4	0.04
MF-600	64.13	29.35	6.52	2.6	1.42	47.9	0.26

[a] Determined by XPS. [b] Determined by EA. [c] Calculated by nitrogen adsorption–desorption test.

Table S7 N species contents and N_{2c}/N_{3c} atomic ratios in melamine-600 and MF-600 by XPS.

Sample	N species and corresponding contents (at.%)			N_{2c}/N_{3c}
	N_{2c}	N_{3c}	NH_x	
melamine-600	74.10 (398.46 eV)	16.76 (400.02 eV)	6.19 (401.07 eV)	4.42
MF-600	63.91 (398.42 eV)	26.19 (400.05 eV)	8.48 (401.06 eV)	2.44

■ C_2H_2 and HCl adsorptions

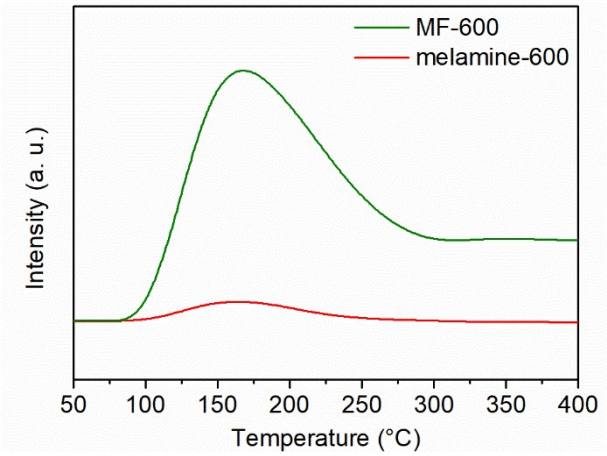

Fig. S8 C_2H_2-TPD of MF-600 and melamine-600 catalysts. C_2H_2-TPD was performed in the temperature range 50–400 °C with a heating rate of 10 °C·min^{-1}.

The C_2H_2-TPD tests on MF-600 and melamine-600 were first conducted, the results are shown in Fig. S8. It is clear that a larger desorption peak of acetylene was observed on MF-600 than melamine-600, meaning a better acetylene adsorption on MF-600 than melamine-600.

For HCl adsorption, however, due to the corrosive nature of HCl gas and the limitations of experimental conditions, the HCl-TPD test was not conducted here. To solve this problem, an alternative experiment was performed on microreactor to investigate the adsorption performance of HCl on MF-600 and melamine-600. The process was controlled as shown in Fig. S9. The sample (MF-600/melamine-600, 0.5 g) was first purged with N_2 (10 mL·min^{-1}) for 1 h at 180 °C to remove residual air and moisture, and then was treated in HCl flow (1 mL·min^{-1}) for 1 h. After that, the treated samples were swept with N_2 (mL·min^{-1}) for another 2 h to remove physisorbed and/or weakly bonded species. Finally, pure C_2H_2 gas (1 mL·min^{-1}) was fed through catalyst layer, the reacted gas mixture was analyzed using an online GC with

a thermal conductivity detector. It can be seen clearly that more VCM was produced over MF-600 than melamine-600, meaning more HCl adsorption on MF-600 than melamine-600.

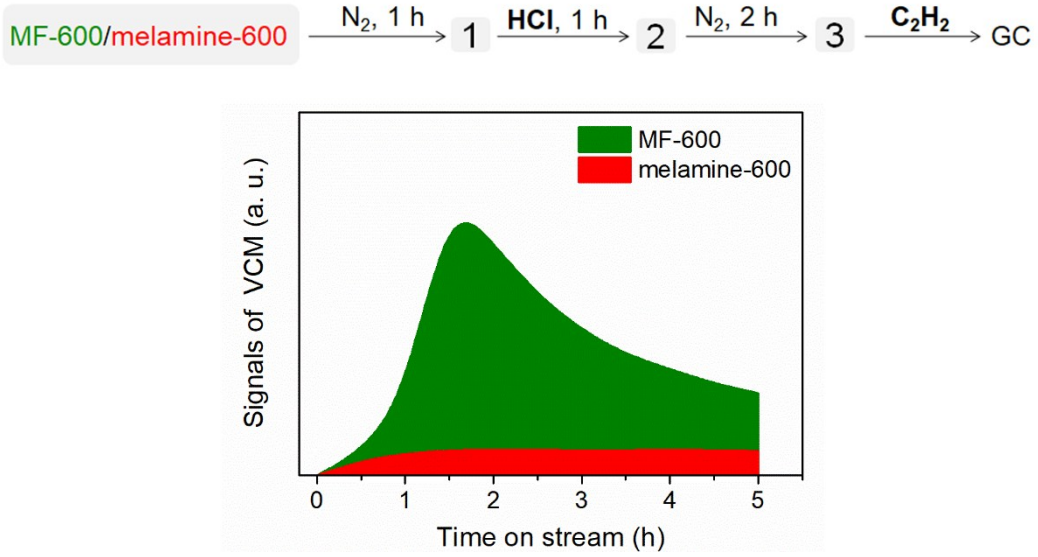

Fig. S9 Signals of VCM detected on GC over MF-600 and melamine-600.

To further explore the adsorption difference of acetylene and HCl on one catalyst, MF-600 was selected for investigation. Based on the experiment for HCl-adsorption conducted in Fig. S9 (**HCl** first then $\mathbf{C_2H_2}$), another treated route ($\mathbf{C_2H_2}$ first then **HCl**) was also carried out for comparation (Fig. S10). It can be seen clearly that more VCM was produced with route A than route B, meaning more HCl adsorption on MF-600 than acetylene.

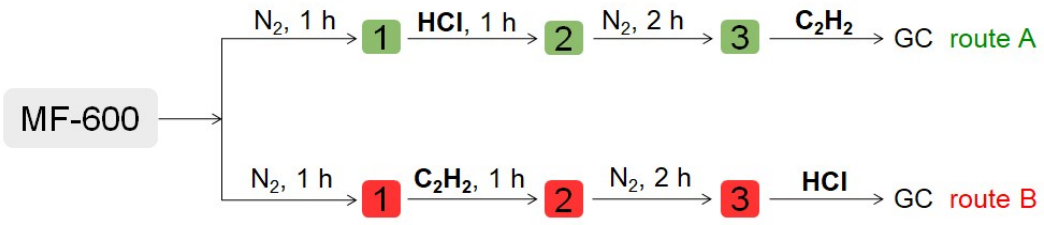

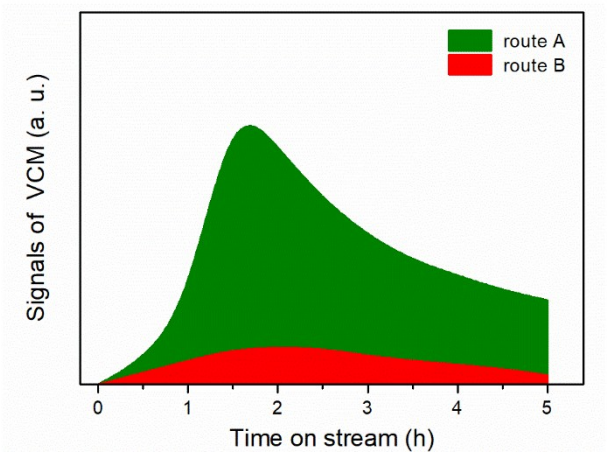

Fig. S10 Signals of VCM detected on GC according to routes A and B with MF-600.

In summary, based on the results of C_2H_2-TPD tests (**Fig. S8)** and contrast experiments (**Fig. S9** and **Fig. S10**), we can conclude that MF-600 had better adsorptions of acetylene and HCl than melamine-600, and at the same time MF-600 had better adsorption of HCl than acetylene.

■ DFT calculations

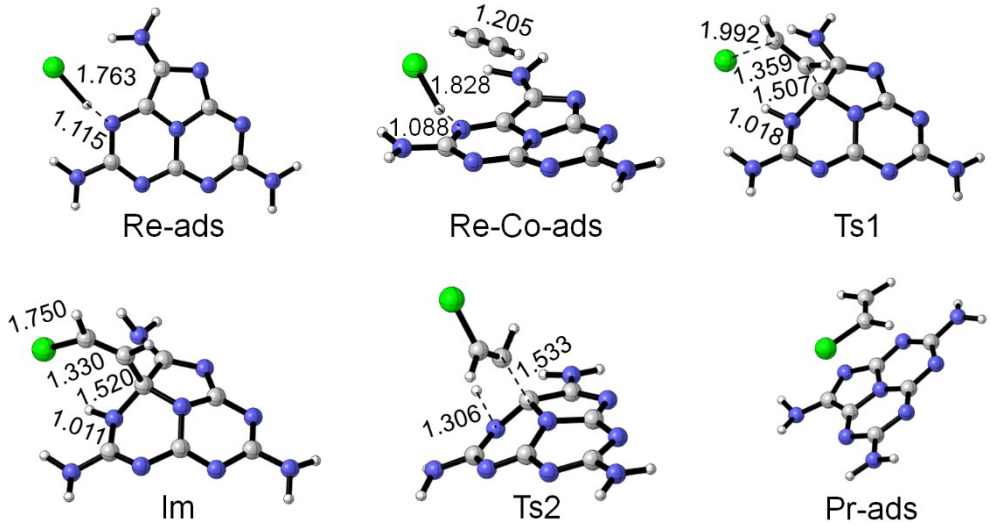

Fig. S11 Optimized geometries of the substances involved in reaction path on F-g-C_3N_4-N1. Re-ads/Co-ads (reactant adsorbed/Co-adsorbed), Pr-ads (product adsorbed), Ts (transition state), Im (intermediate).

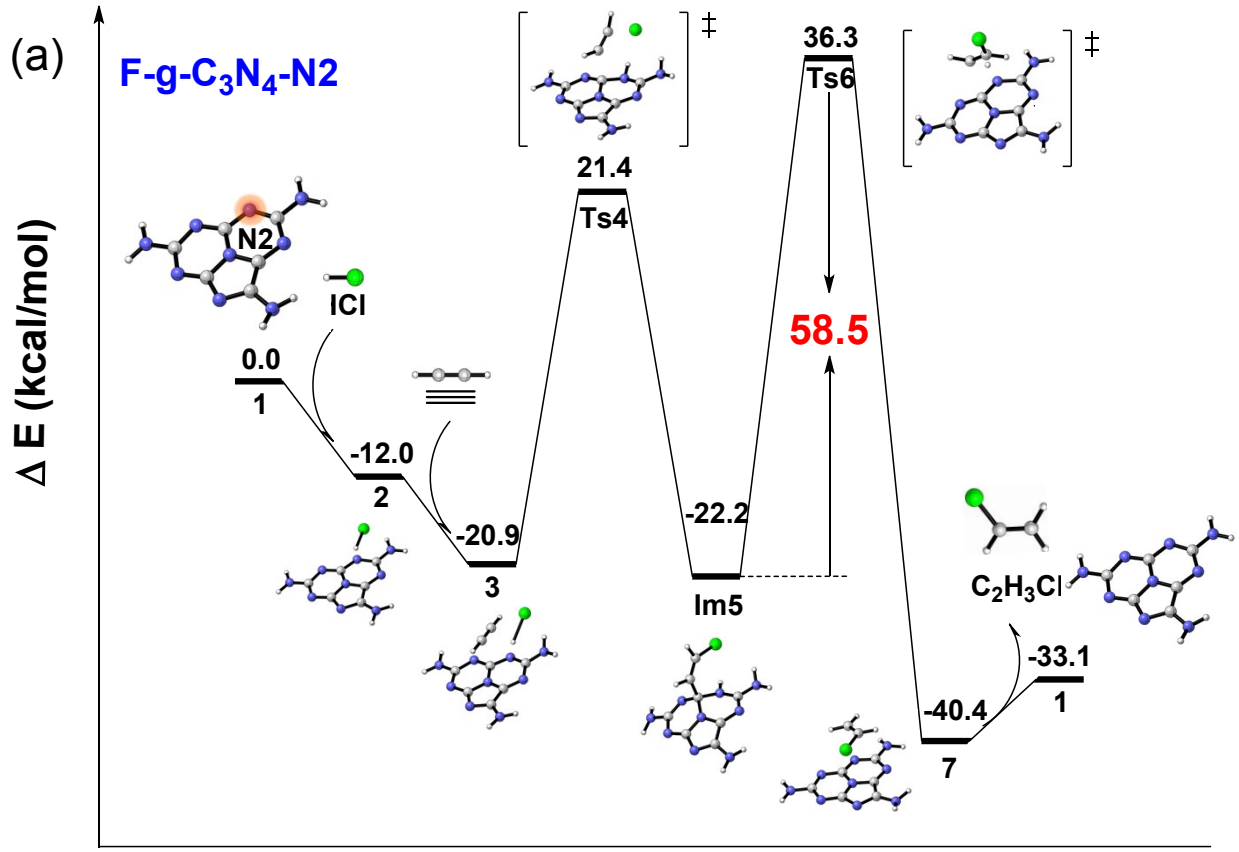
(a)
F-g-C3N4-N2
Δ E (kcal/mol)
N2
ICl
0.0
1
-12.0
2
-20.9
3
21.4
Ts4
-22.2
Im5
36.3
Ts6
58.5
C2H3Cl
-40.4
7
-33.1
1

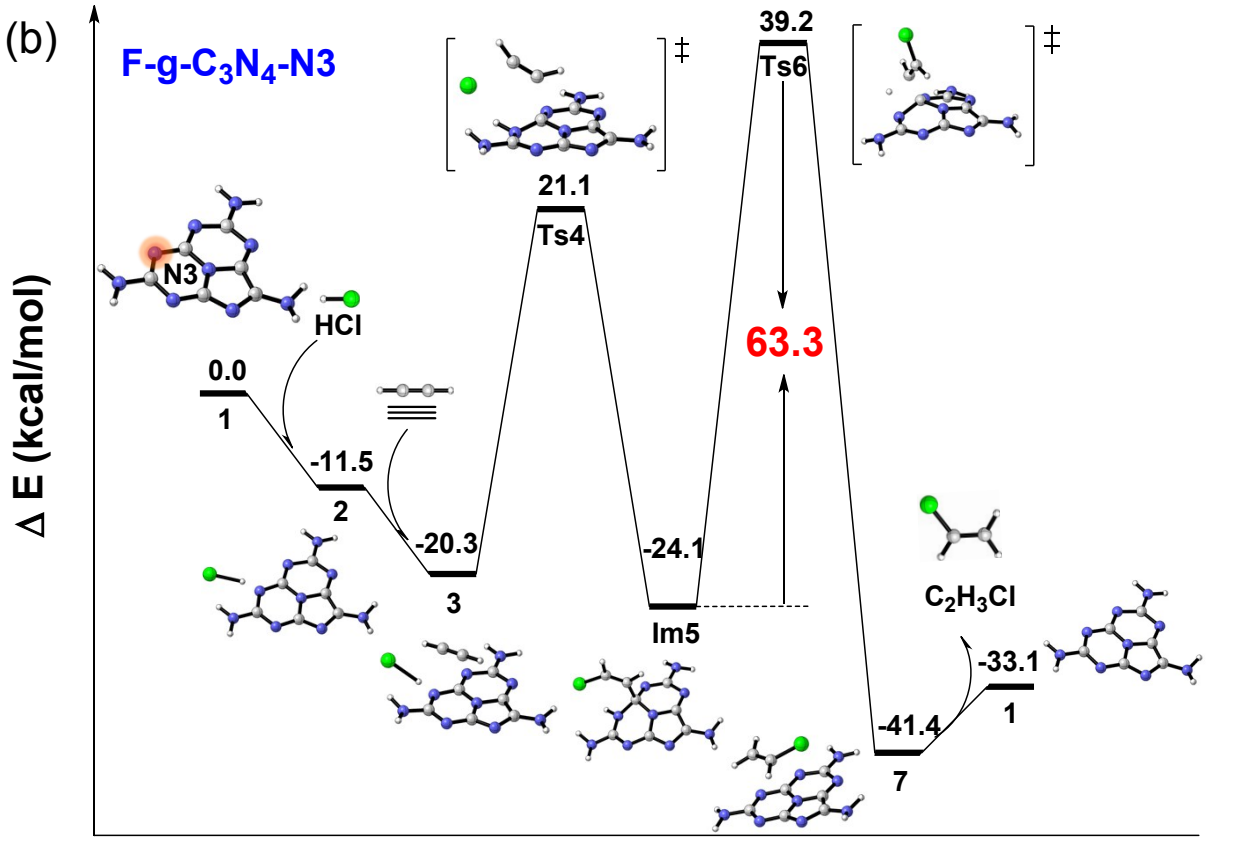
(b)
F-g-C3N4-N3
Δ E (kcal/mol)
N3
HCl
0.0
1
-11.5
2
-20.3
3
21.1
Ts4
-24.1
Im5
39.2
Ts6
63.3
C2H3Cl
-41.4
7
-33.1
1

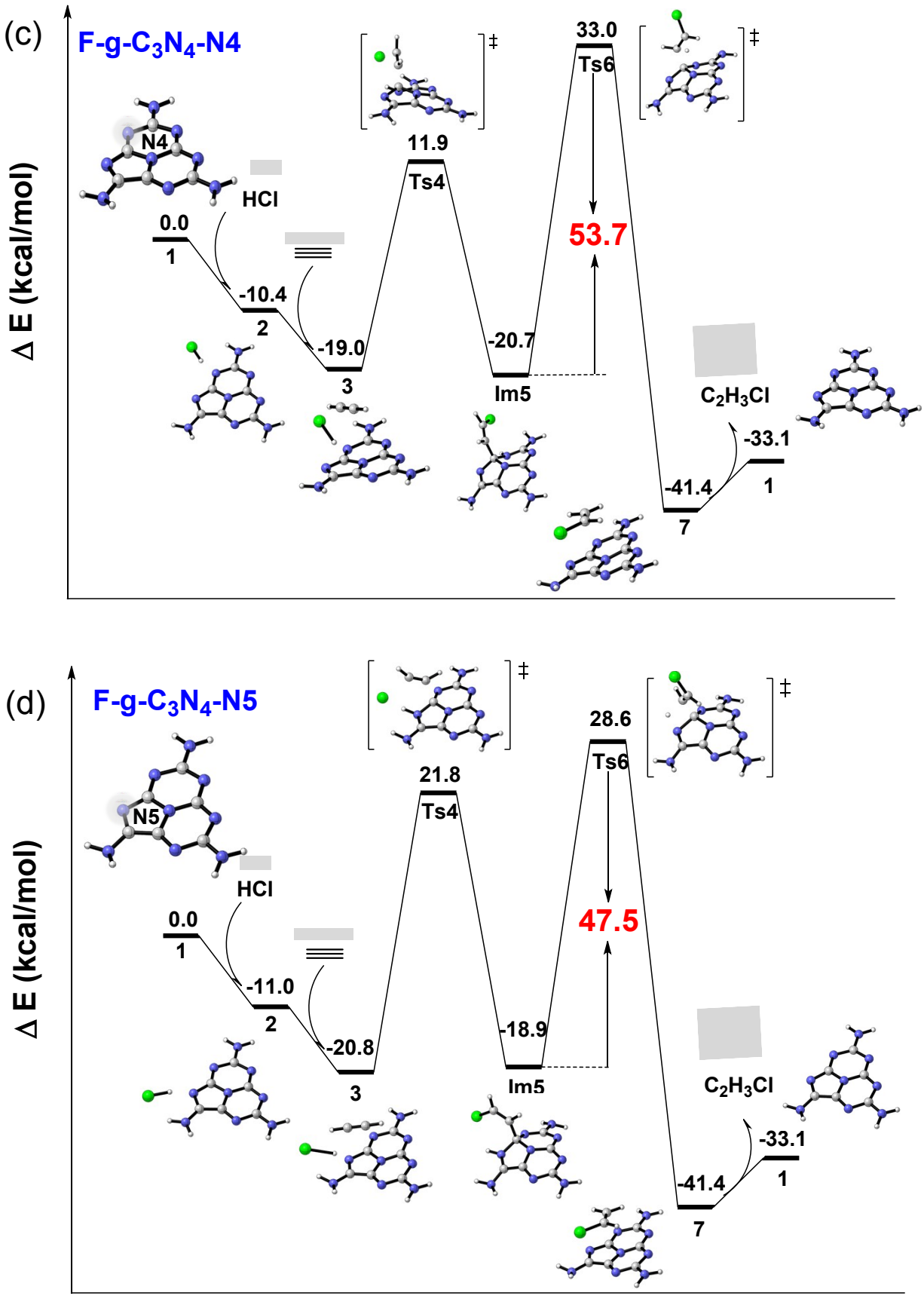

Fig. S12 Reaction energy diagrams of the substances involved in reaction paths on (a) N2, (b) N3, (c) N4, and (d) N5 sites of F-g-C_3N_4.

■ References

[S1] J. Zhao, B. Wang, Y. Yue, G. Sheng, H. Lai, S. Wang, L. Yu, Q. Zhang, F. Feng, Z-T. Hu, X. Li, *J. Catal.,* 2019, 373, 240–249.

[S2] X. Li, Y. Wang, L. Kang, M. Zhu, B. Dai, *J. Catal.,* 2014, 311, 288–294.

[S3] B. Dai, K. Chen, Y. Wang, L. Kang, M. Zhu, *ACS Catal.,* 2015, 5, 2541−2547.

[S4] S. Chao, F. Zou, F. Wan, X. Dong, Y. Wang, Y. Wang, Q. Guan, G. Wang, W. Li, *Sci Rep.,* 2017, 7, 39789.

[S5] X. Li, X. Pan, L. Yu, P. Ren, X. Wu, L. Sun, F. Jiao, X. Bao, *Nat Commun.,* 2014, 5, 3688.

[S6] X. Dong, S. Chao, F. Wan, Q. Guan, G. Wang, W. Li, *J. Catal.,* 2018, 359, 161–170.

[S7] X. Li, P. Li, X. Pan, H. Ma, X. Bao, *Appl. Catal. B: Environ.,* 2017, 210, 116–120.

[S8] C. Zhang, L. Kang, M. Zhu B. Dai, *RSC Adv.,* 2015, 5, 7461–7468.

[S9] P. Li, H. Li, X. Pan, K. Tie, T. Cui, M. Ding, X. Bao, *ACS Catal.,* 2017, 7, 8572−8577.